Nonlinear Insulator in Complex Oxides

Z. Q. Liu[1,2], D. P. Leusink[1,2], W. M. Lü[1,3], X. Wang[1,2], X. P. Yang[4], K. Gopinadhan[1,3]

A. Annadi[1,2], S. Dhar[1,3], Y. P. Feng[2], H. B. Su[4], G. Xiong[1,3], T. Venkatesan[1,2,3],

Ariando[1,2*]

[1]*Nanocore,* [2]*Department of Physics,* [3]*Department of Electrical and Computer*

Engineering, National University of Singapore, Singapore

[4]*Division of Materials Science, Nanyang Technological University, Singapore*

*To whom correspondence should be addressed.
E-mail: ariando@nus.edu.sg

Here we report a new class of material which we have coined as "nonlinear

insulators" that exhibit a reversible electric-field-induced metal-insulator transition.

We demonstrate this behaviour for an insulating LaAlO₃ thin film in a

metal/LaAlO₃/Nb-SrTiO₃ heterostructure. Our experimental results exclude the

possibility of diffusion of the metal electrodes or oxygen vacancies into the LaAlO₃

layer. Instead, the phenomenon is attributed to the formation of a quasi-conduction band (QCB) in the defect states of $LaAlO_3$ that forms a continuum state with the conduction band of the Nb-$SrTiO_3$. Once this continuum (metallic) state is formed, the state remains stable even when the voltage bias is turned off. An opposing voltage is required to deplete the charges from the defect states.

The insulating state is one of the most basic electronic phases in condensed matter. This state is characterized by an energy gap for electronic excitations that makes an insulator electrically inert at low energy. However, for complex oxides, the very concept of an insulator must be re-examined. Complex oxides behave differently from conventional insulators such as SiO_2, on which the entire semiconductor industry is based, because of the presence of multiple defect levels within their bandgap.

The electronic state of complex oxides can be changed by chemical doping, temperature, external pressure (*1-3*), magnetic fields (*4*), electric fields (*5*) or light (*6*). In particular, the electric field-induced metal-insulator transition (MIT) has attracted a lot of attention because of its intriguing physical mechanisms (*7, 8*) and potential for device applications. With the recent excitement in resistive switching (*9-11*) in a typical metal/insulator/metal structure (*12, 13*), electric-field-induced MIT has been revisited as a possible mechanism (*14-16*). A number of different mechanisms (*17-20*) have been previously demonstrated for resistive switching, such as electric-field-induced oxygen vacancy migration resulting in the formation of conducting filaments (*17, 18*), and reversible metal migration from electrodes (*19*). Such a variety of field-induced phenomena arise from the complex defects that are present in these oxides. Cationic and anionic defects can form trap states

within the bandgap of even wide bandgap oxides, drastically affecting their insulating

properties (*21*). In this letter, we show a reversible metal-insulator transition caused by

the electrical population of defect levels in the bandgap of oxide insulators, which in turn

can play a crucial role in determining the (nonlinear) insulating nature of the material.

The very large bandgap of $LaAlO_3$, ~5.6 eV (*22*), and the possibility of fabricating high

crystalline quality $LaAlO_3$ thin films make it an ideal material for investigation of the

nonlinear insulating properties of complex oxides.

Typical metal/$LaAlO_3$/Nb-$SrTiO_3$ structures (Fig. 1A) with different top electrodes (Cu

or Au) and different $LaAlO_3$ layer thicknesses of 25, 50 and 150 nm were prepared

(supplementary information). Figure 1 shows that the electronic phase of the Cu/$LaAlO_3$

(150 nm)/Nb-$SrTiO_3$ structure can be reversibly changed by the applied voltages. In the

following, we will describe the switching sequence starting with the negative voltage.

The temperature dependence of the sample resistance (*R-T*) curve of the initial state

indicates typical insulating behaviour (Fig. 1B) that corresponds to the initial current-

voltage (*I-V*) curve of the system (from i to j in Fig. 1C).At low voltages, the resistance is

very high but when the voltage reaches –6.8 V, a sharp jump in the current is seen (Fig.

1C). Because of the imposed compliance current of 0.1 A, which is used to prevent

sample damage (*12, 19*), the current saturates at 0.1 A. As the voltage is scanned back to

0 V, a linear *I-V* characteristic is seen, which corresponds to a stable metallic state (inset

m in Fig. 1C). Hence, upon the dramatic switching of the resistive state triggered at −6.8

V, the resistance changes from ~14 MΩ to ~25 Ω at room temperature, which is

concomitant with a phase transition from the insulating to the metallic phase. The

metallic state persists until the positive voltage scan reaches about 2.4 V; at that level, the

structure transitions into a high-resistance (n-o-p-q in Fig. 1C) and non-metallic (inset q

in Fig. 1C) state. The reversible phase transition is reproducible, as shown in the second

I-V cycle (Fig. 1D). These behaviours are totally unexpected for a wide bandgap insulator

such as $LaAlO_3$.

The anomalous insulating behaviour of $LaAlO_3$ cannot be explained by artefacts such as

anodization or redox of the active metal electrodes (*19*). In those cases, anodic dissolution

of the metal electrode is possible only if adequate positive voltage is applied to an active

metal electrode, and the resulting cations can be driven by the strong electric field into

the insulating film where they form metallic filaments. To further eliminate this

possibility, structures with inactive Au as the top electrode material were prepared and

analysed; these structures showed no observable difference in their resistive switching

behaviour compared to those that had Cu as the top electrode (supporting online material).

This strongly suggests that the reversible phase transition cannot be caused by the

diffusion of metal electrodes.

Another possible mechanism for this anomalous insulating phenomenon is the migration

of oxygen vacancies. If such a mechanism is occurring, the applied electric field could

only change the distribution of the positively charged oxygen vacancies (23). Therefore,

no insulating phase would appear, even at higher resistance states. Our case is also

significantly distinct from the type of resistive switching that originates from the electro-

migration of excess oxygen as described by Shi *et al.* (24); in that experiment, the

resistive switching disappeared at low temperatures because of the low diffusion

coefficient of the oxygen. To verify this, the low temperature switching properties were

examined using the same structure with a Au electrode. The initial insulating state of this

structure is shown in the inset i of Fig. 2A. After cooling to 4.1 K, the *I-V* measurements

were performed and the structure was negatively biased to −8.8 V, at which it switched to

a linear state (Fig. 2A) with a very small resistance of ~12 Ω, which corresponds to a

metallic phase (inset n in Fig. 2A). The voltage required to obtain this switching is larger

than the one at room temperature. The sample was then warmed up to 298 K, after which

it was switched back to a non-metallic state (inset m in Fig. 2B) with a higher resistance

of ~10 kΩ. These results are consistent with the results seen in the room-temperature

device; thus, it is very difficult to attribute the nonlinear insulating properties observed in

$LaAlO_3$ to the oxygen vacancy or excess oxygen scenarios.

We propose a novel mechanism to describe this nonlinear insulating behaviour. In Fig.

3A, a sketch of the band structure of the device is depicted. Our Femtosecond pump-

probe experiments on single crystal $LaAlO_3$ reveal that defect states can exist in $LaAlO_3$

within a wide energy range at approximately 2.0 eV below the conduction band, which is

consistent with the theoretical calculations of Luo *et al.* (*25*). Initially, there is no

conduction between the Nb-$SrTiO_3$ and $LaAlO_3$. Under negative bias, charges will be

injected into and fill up the $LaAlO_3$ defect levels. At the voltage where a dramatic

conductivity transition is seen, the electron population of the defect levels is high enough

to form a metallic state. We call this defect-mediated conduction band a "quasi-

conduction band" (QCB). Once the energy level of QCB lines up (Fig. 3B) with the

Fermi level of Nb-$SrTiO_3$, which is slightly above its conduction band (*26*), a continuum

state is established, and this state remains even when the current is reduced to zero

because of the overlap of the electron wave functions. The effective charge transferred to

7

the defect levels at the switching threshold of 0.22 A is estimated to be around 4.6×10^{19} cm^{-3} for a device area of 0.02 cm^2, a LaAlO$_3$ thickness of 150 nm and a defect level lifetime of ~10 microseconds. While this carrier concentration is about 3.5 times smaller than that of the Nb-SrTiO$_3$, which is 1.6×10^{20} cm^{-3}, it makes the LaAlO$_3$ a stable metallic system. To validate this idea, theoretical calculations on interstitial La^{2+} defect of LaAlO$_3$ and percolation of wave functions were performed (supporting online material). It was found that the charge density higher than 0.011872 $Å^{-3}$ exists mainly at La atoms around the defect with strong d-orbital character, which is of the same order of magnitude as our estimated number. Interestingly, the charge density of the lowest unoccupied conduction band at Γ point around Ti atoms in cubic SrTiO$_3$ has the same magnitude as that of the defect state of LaAlO$_3$ (Fig. 3D) such that the defect La-d and Ti-d wave functions can couple if they are in proximity. The most interesting aspect of the QCB is the inherent hysteresis; the only way that this device can be restored to the original insulating state is by applying an opposing voltage, which will then remove the carriers from the QCB (Fig. 3C). Intriguingly, the transition where the system becomes an insulator (with an applied positive voltage) is close to 2.4 V, which is the difference in the bandgaps of LaAlO$_3$ and Nb-SrTiO$_3$.

To explore the dependence on the sequence of polarity switches, an initial positive

voltage scan was conducted (Fig. 4A). There was no current until a threshold was reached

at about 1 V, beyond which the current increased to a maximum and then decreased until

the system went back to the original resistive state. This switching behaviour can be

understood by considering the same defect model but with the electrons being pumped

into the defect states from the valence band side. At the same time, the position of the

Nb-SrTiO$_3$ conduction band is pushed down with respect to the LaAlO$_3$ band and at

about 1 V the defect band has enough charge to overlap with it (to form a QCB), which

leads to a stable metallic state as depicted in Fig. 4B. However, as the positive voltage is

increased, the electrons in the QCB will be pumped into the conduction bands of LaAlO$_3$

and the metal electrode and the Nb-SrTiO$_3$ conduction band will be further pushed down;

this leads to a lack of overlap between the bands and thus the original resistive state (Fig.

4C).

This QCB originates from the defect levels in the bandgap of LaAlO$_3$. To test this

hypothesis, devices with very thin LaAlO$_3$ films (25 and 50 nm), which are likely to have

fewer defects, were examined, and no switching at all was observed (supporting online

material). The defect model is also validated by the change in resistive state values after

9

several cycles; the device has slightly lower resistance values after the first cycle, and

those values slightly increase in the later cycles as shown in Fig. 1, C and D. This change

points to the possibility of defect production and defect rearrangement after large currents

have passed through these devices, which supports the defect-mediated QCB model for

nonlinear insulating $LaAlO_3$.

Most of the complex oxides have predominantly ionic bonds and are prone to a variety of

cationic and anionic defects including vacancies, interstitials and antisites. These defects

create a plethora of electronic states within the bandgap of these oxides and constitute a

new class of materials that we have coined as "nonlinear insulators". In these insulators,

the defect levels can be populated to form QCBs, which can lead to multiple conduction

states in the same system. These states can be stabilised if an adjacent metallic

conduction band overlaps with them. The only way to restore the levels back to their

original state is by removing the carriers from the defect levels; this phenomenon is what

leads to hysteresis in the *I-V* curves.

The implications of these nonlinear insulators are far-reaching. For example, the use of

multi-component oxides as insulators in devices (*e.g.,* high-*k* dielectrics in silicon CMOS

devices) must be exercised with caution. However, once the defect states in these

materials can be controlled, researchers will be in a position to develop many novel

device concepts based on these non-linear insulators.

References and Notes:

1. M. Imada, A. Fujimori, Y. Tokura, Metal-insulator transitions. *Rev. Mod. Phys.* **70**, 1039-1263 (1998).

2. P. Limelette *et al.,* Universality and critical behavior at the Mott transition. *Science* **302**, 89-92 (2003).

3. D. B. McWhan, T. M. Rice, Critical pressure for the metal-semiconductor transition in V_2O_3. *Phys. Rev. Lett.* **22**, 887-890 (1969).

4. H. Kuwahara, Y. Tomioka, A. Asamitsu, Y. Moritomo, Y. Tokura, A first-order phase-transition induced by a magnetic field. *Science* **270**, 961-963 (1995).

5. T. Murakami, J. Sakai, S. Imai, Electric-field-induced insulator-metal transition in $Pr_{0.5}Ca_{0.5}MnO_3$ thin films in ramp-type junctions. *J. Appl. Phys.* **94**, 6549-6551 (2003).

6. S. Shamoto *et al.,* Light-induced metal-insulator transition in $Lu_2V_2O_7$. *J. Phys. Chem. Solids* **62**, 325-329 (2001).

7. R. Ugajin, Electric-field-induced Mott metal-insulator transition. *Phys. Rev. B* **53**, 10141-10147 (1996).

8. R. Y. Gu, Z. D. Wang, C. S. Ting, Theory of electric-field-induced metal-insulator transition in doped manganites. *Phys. Rev. B* **67**, 1531011-1531014 (2003).

9. A. Asamitsu, Y. Tomioka, H. Kuwahara, Y. Tokura, Current switching of resistive states in magnetoresistive manganites. *Nature* **388**, 50-52 (1997).

10. S. Q. Liu, N. J. Wu, A. Ignatiev, Electric-pulse-induced reversible resistance change effect in magnetoresistive films. *Appl. Phys. Lett.* **76**, 2749-2751 (2000).

11. A. Beck, J. G. Bednorz, Ch. Gerber, C. Rossel, D. Widmer, Reproducible switching effect in thin oxide films for memory applications. *Appl. Phys. Lett.* **77**, 139-141 (2000).

12. R. Waser, M. Aono, Nanoionics-based resistive switching memories. *Nature Mater.* **6**, 833-840 (2007).

13. A. Sawa, Resistive switching in transition metal oxides. *Mater. Today* **11**, 28-36 (2008).

14. M. J. Rozenberg, I. H. Inoue, M. J. Sánchez, Nonvolatile memory with multilevel switching: A basic model. *Phys. Rev. Lett.* **92**, 178302 (2004).

15. T. Oka, N. Nagaosa, Interfaces of correlated electron systems: Proposed mechanism for colossal electroresistance. *Phys. Rev. Lett.* **95**, 266403 (2005).

16. M. J. Rozenberg, I. H. Inoue, M. J. Sánchez, Strong electron correlation effects in nonvolatile electronic memory devices. *Appl. Phys. Lett.* **88**. 033510 (2006)

17. B. J. Choi *et al*., Resistive switching mechanism of TiO_2 thin films grown by atomic-layer deposition. *J. Appl. Phys*. **98**, 033715 (2005).

18. D. -H. Kwon *et al*., Atomic structure of conducting nanofilaments in TiO_2 resistive switching memory. *Nat. Nanotechnol*. **5**, 148-153 (2010).

19. R. Waser, R. Dittmann, C. Staikov, K. Szot, Redox-based resistive switching memories-nanoionic mechanisms, prospects, and challenges. *Adv. Mater.* **21**, 2632-2663 (2009).

20. Y. Chen, L. Chen, G. Lian, G. Xiong, Resistance and superconductivity switching caused by carrier injection: Evidences of self-trapping carriers in oxide electronics. *J. Appl. Phys.* **106**, 023708 (2009).

21. D. Muñoz Ramo, A. L. Shluger, J. L. Gavartin, G. Bersuker, Theoretical prediction of intrinsic self-trapping of electrons and holes in monoclinic HfO_2. *Phys. Rev. Lett.* **99**, 155504 (2007).

22. S. -G. Lim *et al.,* Dielectric functions and optical bandgaps of high-*k* dielectrics for metal-oxide-semiconductor field-effect transistors by far ultraviolet spectroscopic ellipsometry. *J. Appl. Phys.* **91**, 4500-4505 (2002).

23. M. Janousch *et al.,* Role of oxygen vacancies in Cr-doped $SrTiO_3$ for resistance-change memory. *Adv. Mater.* **19**, 2232-2235 (2007).

24. J. P. Shi, Y. G. Zhao, H. J. Zhang, H. F. Tian, X. P. Zhang, Oxygen electromigration induced nonvolatile resistance switching at Ag/La$_2$CuO$_{4+x}$ interface. *Appl. Phys. Lett.* **94**, 192103 (2009).

25. X. Luo, B. Wang, Y. Zheng, First-principles study on energetics of intrinsic point defects in LaAlO$_3$. *Phys. Rev. B* **80**, 104115 (2009).

26. X. G. Guo *et al.,* Electronic band structure of Nb doped SrTiO$_3$ from first principles calculation. *Phys. Lett. A* **317**, 501-506 (2003).

27. The authors would like to thank Y. L. Zhao and M. Yang for experimental support and the National Research Foundation (NRF) Singapore under the Competitive Research Program "Tailoring Oxide Electronics by Atomic Control" for financial support.

Figure legends:

Fig. 1. Demonstration of a nonlinear insulator. (**A**) Sample configuration and measurement geometry. (**B**) R-T curve of the initial resistance state for Cu/LaAlO$_3$ (~150 nm)/Nb-SrTiO$_3$ structure on a semi-logarithmic scale. (**C**) I-V measurements by scanning voltage along 0 → -7 V → 0→ 7 V → 0 and R-T curves of different resistance states. The inset m and inset q are the R-T curves after scanning the voltage through points m and q to zero, respectively. The horizontal data between points k and l are due to the compliance current in action. (**D**) I-V curves after the cycle shown in **C** and R-T curves of different resistance states. The inset l and inset p are the R-T curves after scanning the voltage through points l and p to zero, respectively.

Fig. 2. Low temperature switching. (**A**) Negative switching of Au/LaAlO$_3$ (~150 nm)/Nb-SrTiO$_3$ at 4.1 K. (Inset i) R-T curve of the initial state. (Inset n) R-T curve after negatively scanning voltage back to 0, *i.e.*, after 0 → -10 V → 0 at 4.1 K. The current values in the k-l-m sequence are confined by the compliance current. (**B**) Positive scan after **A** at 298 K by 0 → 7 V → 0. (Inset) R-T curve after positive scan.

Fig. 3. Schematics of QCB. (**A**) Schematic of the band diagram of the device with no voltage bias. The middle defect band represents the defect levels of LaAlO$_3$, which are widely distributed in the bandgap at ~2 eV below the conduction band. (**B**) Formation of a QCB under an initial negative voltage bias. (**C**) Depletion of electrons in the QCB by a subsequent positive bias. (**D**) Partial charge density distributions of local defect state around the Fermi level for LaAlO$_3$ and lowest unoccupied conduction band at Γ point for cubic SrTiO$_3$, respectively. The yellow clouds represent charge densities exceeding 0.011872 electrons/$\mathring{A}^3$.

Figure 4: Switching polarity. (**A**) *I-V* characteristics of the initial positive voltage scan for Cu/LaAlO$_3$ (~150 nm)/Nb-SrTiO$_3$ structure from 0 → 7 V → 0 following the sequence i-j-k-l-m-n. The inset shows the *R-T* curve after scanning the voltage back to zero. (**B**) Pumping of electrons from the valence band of LaAlO$_3$ by an initial positive bias greater than 1 eV. (**C**) Generation of a band offset between the QCB and the Nb-doped SrTiO$_3$ conduction band by a subsequent increase in the positive bias.
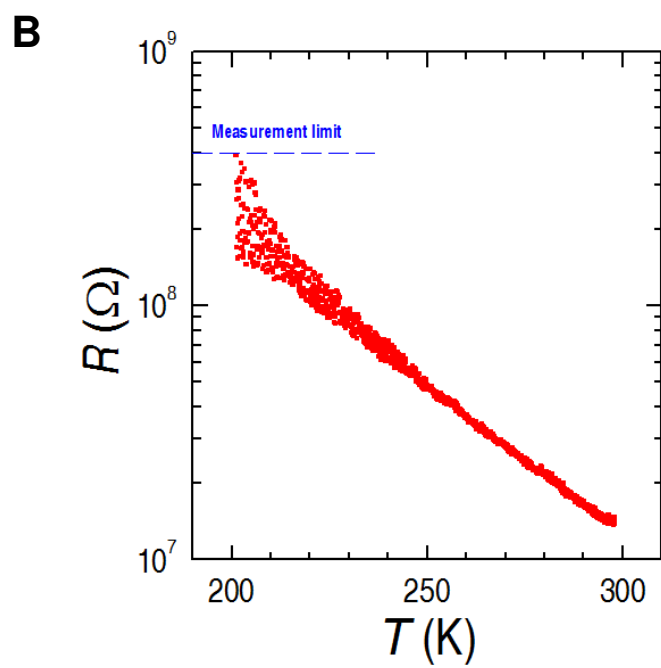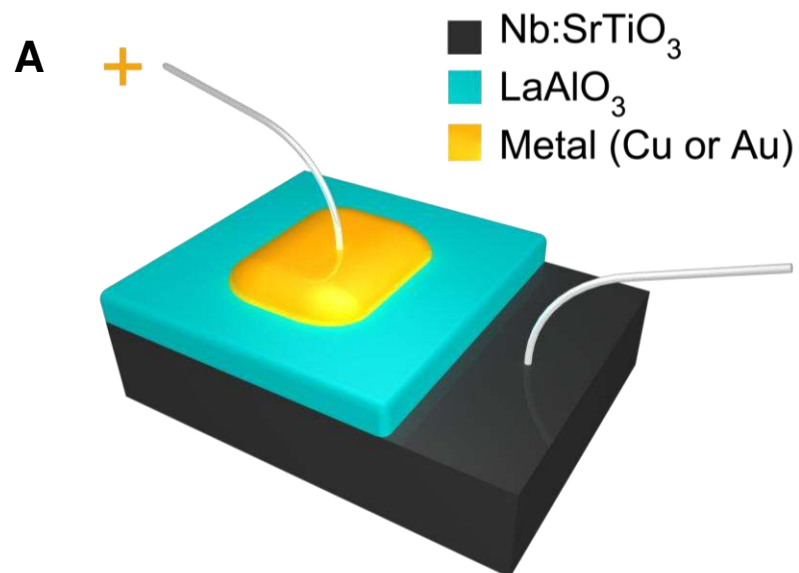
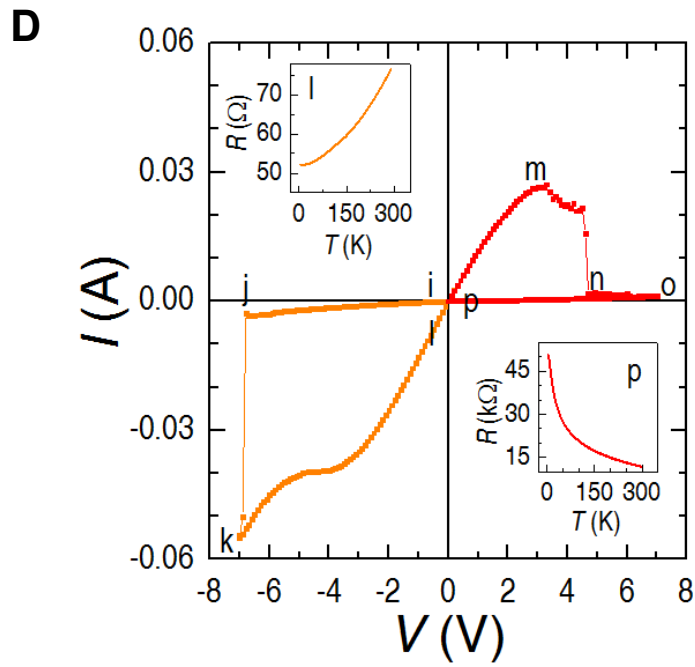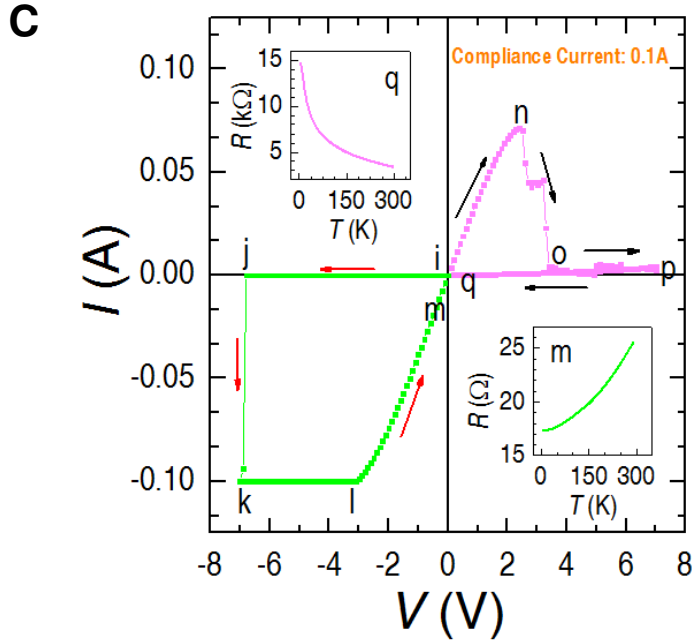**Fig. 1., Liu** *et al.*

Fig. 1., Liu *et al.*

C

D

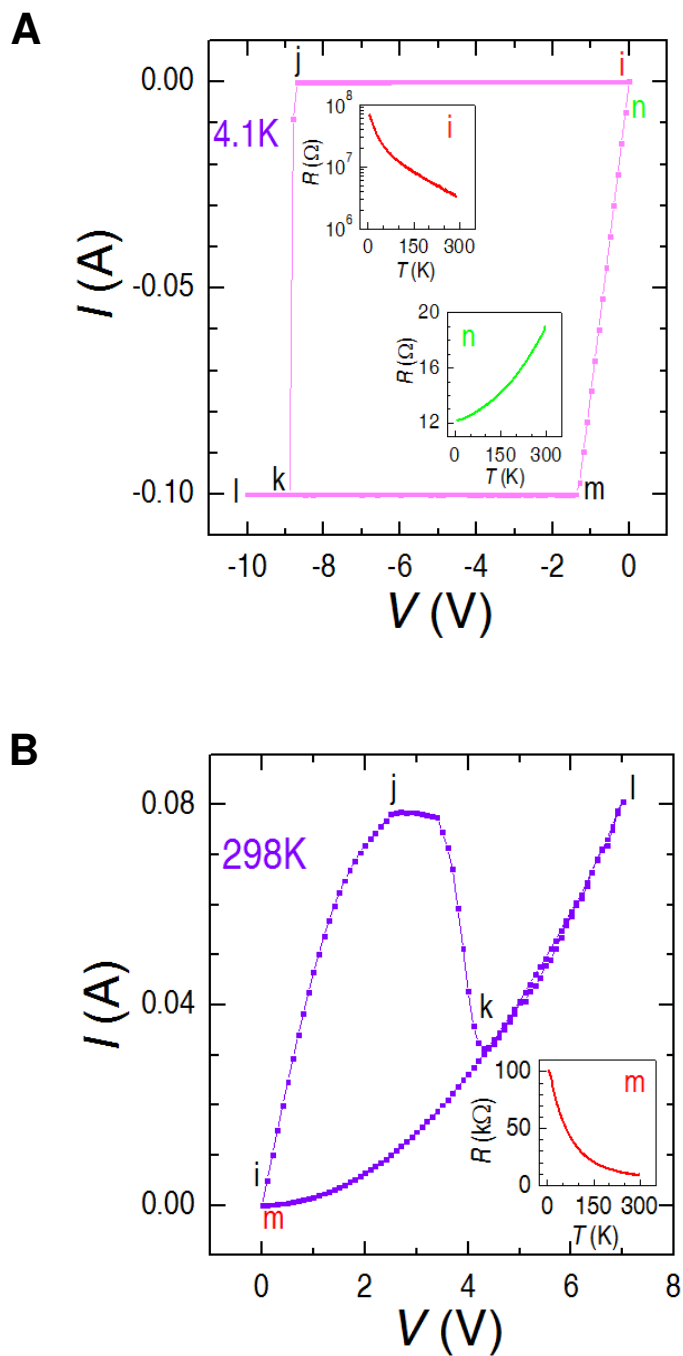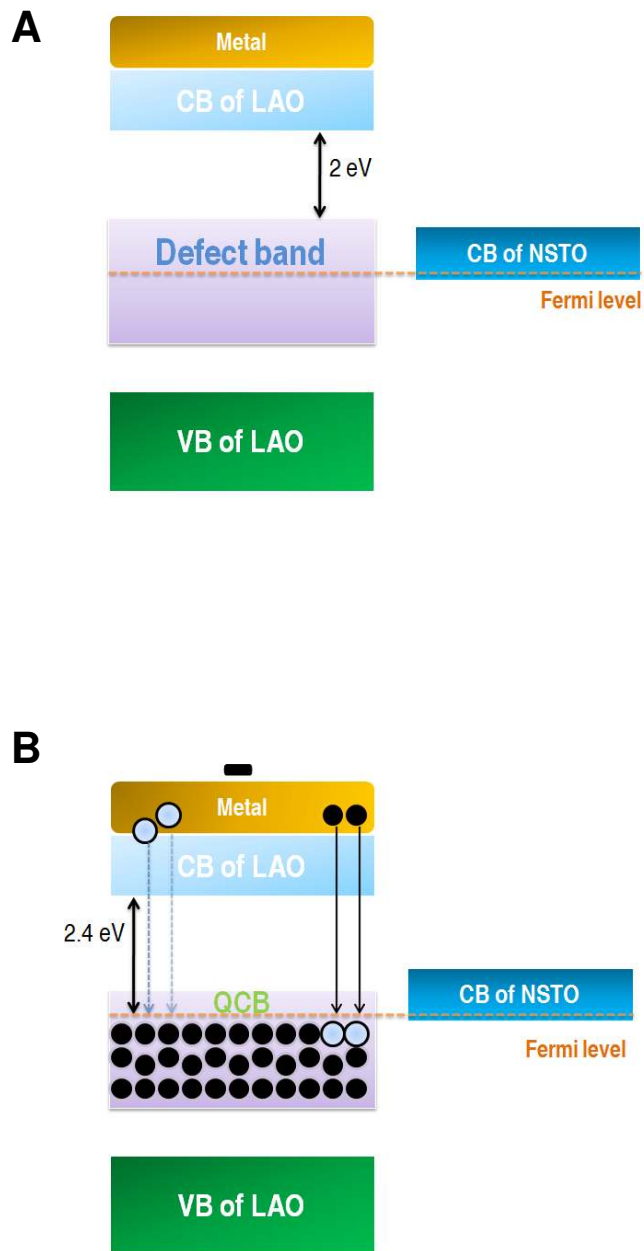**Fig. 2., Liu *et al.***

A

B

Fig. 3., Liu *et al.*

Fig. 3., Liu *et al.*

Fig. 4., Liu *et al.*